

# Accelerating Graph-based Tracking Tasks with Symbolic Regression

Nathalie Soybelman<sup>1</sup>, Carlo Schiavi<sup>2</sup>, Francesco A. Di Bello<sup>2</sup>,  
Eilam Gross<sup>1</sup>

<sup>1</sup> Weizmann Institute of Science, Israel

<sup>2</sup> University of Genova and INFN Sezione di Genova, Italy

E-mail: [nathalie.soybelman@weizmann.ac.il](mailto:nathalie.soybelman@weizmann.ac.il)

April 2024

**Abstract.** The reconstruction of particle tracks from hits in tracking detectors is a computationally intensive task due to the large combinatorics of detector signals. Recent efforts have proven that ML techniques can be successfully applied to the tracking problem, extending and improving the conventional methods based on feature engineering. However, complex models can be difficult to implement on heterogeneous trigger systems, integrating architectures such as FPGAs. Deploying the network on an FPGA is feasible but challenging and limited by its resources. An efficient alternative can employ symbolic regression (SR). We propose a novel approach that uses SR to replace a graph-based neural network. Substituting each network block with a symbolic function preserves the graph structure of the data and enables message passing. The technique is perfectly suitable for heterogeneous hardware, as it can be implemented more easily on FPGAs and grants faster execution times on CPU with respect to conventional methods. We note that while the tracking problem is the target for this work, it also provides a proof-of-principle for the method that can be applied to many use cases.

*Keywords:* graph neural networks, object condensation, symbolic regression

## 1. Introduction

In High Energy Physics experiments, such as ATLAS [1] and CMS [2], operating at LHC [3], data collection relies on sophisticated trigger systems [4–7] that select interesting events and reject others to reduce the amount of data to be stored significantly. Inner tracking detector data, consisting of hits produced by the passage of charged particles, is crucial for triggering as it contains valuable event information. The

task of track reconstruction from hits is challenging due to combinatorics of detector signals and, therefore, ranks among the top time-consuming trigger tasks [8]. With upcoming upgrades for the High Luminosity LHC, the instantaneous luminosity and the number of simultaneous collisions per bunch crossing (pile-up) will increase respectively by a factor of 4 and 8, reaching unprecedented heights. Major changes and improvements to the data acquisition pipelines are indispensable for data taking.

Many machine-learning (ML) algorithms were explored and investigated to improve on classical track reconstruction approaches in the context of the *TrackML* challenge [9, 10] and beyond. Most promising approaches are based on graph-neural networks [11–17] as they offer a natural way of representing and processing the tracking data.

A full deployment of these methods, denoted by large memory requirements and non-negligible execution times, into the ATLAS and CMS trigger strategies is still an open project. Currently, both trigger systems can perform tracking only in the software-based high-level trigger (HLT), still largely relying on CPU farms. The use of GPUs has only recently been introduced in CMS to offload a part of the tracking task [18], but its potential is not yet fully exploited. Also, it is considered important to explore alternative approaches based on heterogeneous hardware solutions in parallel, including adopting Field Programmable Gate Arrays (FPGAs).

Speeding up the inference of ML tools by incorporating quantization and implementing them on FPGAs [19–23] could also allow extending the scope of tracking to the hardware-based early stages of the trigger selection [24]. That approach can include GNNs or transformer architectures, as shown in [25–28]; nevertheless, this works for rather small and simple networks ( $\mathcal{O}(10\text{k})$  parameters) but not for large-scale GNNs due to memory limitations.

Alternatively, symbolic regression can replace or approximate a dense neural net with an analytical function. Such studies were performed in [29–31] to find more interpretable and physics-motivated expressions. It can also be used to accelerate inference time and ease implementation on FPGAs without much loss in performance, as was investigated in [32].

In this work, we propose a novel extension of such a method, using symbolic regression to approximate a graph neural network for track finding. This cannot be done straightforwardly as the network input is not a given list of variables but a set of objects with properties without a fixed cardinality. Therefore, it is impossible to have a single analytical function that takes the hits as input and gives tracks as output. Instead, we take the building blocks of the network, which are dense layers, and fit them separately with a symbolic expression. That way, the data’s graph structure and the message-passing mechanism are preserved. This leaves room for flexibility, allowing the replacement of the full GNN or a subset of its building blocks, keeping the remaining ones as neural nets.

As a test bench for this approach, we developed an algorithm to cluster hits originating from high transverse momentum tracks, distinguishing them from hits produced by soft background tracks and detector noise. The clustered signal hits can be further processed to extract track parameters with a fit procedure.

To perform a proof-of-concept study on the proposed methods, we designed a simplified toy data simulator, allowing a direct comparison between the clustering GNN performance and the one obtained with approximated symbolic regression.

## 2. Dataset

The toy data generator adopted for this study considers a cylindrical detector composed of 8 concentric layers. Its geometry follows the barrel ATLAS Inner Detector, with layer radii matching the ones in the Pixel and SCT (SemiConductor Tracker) subdetectors, each consisting of 4 layers. The emulated detector is immersed in a 2 T constant solenoidal magnetic field aligned with the beam axis, approximating the ATLAS experiment setup.

In the following, the coordinate system follows the one adopted in ATLAS and CMS<sup>‡</sup>.

The generator follows the trajectories of simulated charged tracks in the detector volume and calculates their intersection with the detectors to create hits. To keep the model simple, no interaction of particles with the detector is considered.

To account for experimental resolution effects, the  $\phi$  and  $z$  coordinates of the hits are smeared based on the pitch of the emulated detector sensors. No smearing is applied on the  $r$  coordinate.

Optionally, an average hit inefficiency can be randomly applied for each individual detector layer; in the study presented here, all layers are considered fully efficient.

The signal targeted in this study is a sample of single tracks coming from a simulated hard scatter vertex with  $p_T > 20$  GeV. Tracks are generated in the  $|\eta| < 1.4$  region to be sure they are fully contained in the detector volume, thus avoiding acceptance effects on the corresponding hits.

To emulate the typical beamspot shape in LHC running conditions, each track originates from a primary vertex (PV) whose position along the beam axis is sampled from a Gaussian distribution centred on the axis origin and with a  $\sigma = 5$  cm. The longitudinal ( $z_0$ ) impact parameter, evaluated with respect to the PV, is randomly extracted from a Gaussian distribution centred at 0 and with  $\sigma = 100$   $\mu\text{m}$ ; the transverse ( $d_0$ ) impact parameter is instead always set to 0.

<sup>‡</sup> We adopt a right-handed coordinate system with its origin at the nominal interaction point (IP) in the centre of the detector and the  $z$ -axis along the beam pipe. The  $x$ -axis points from the IP to the centre of the accelerator ring, and the  $y$ -axis points upwards. Polar coordinates  $(r, \phi)$  are used in the transverse plane,  $\phi$  being the azimuthal angle around the  $z$ -axis. The pseudorapidity is defined in terms of the polar angle  $\theta$  as  $\eta = -\ln \tan(\theta/2)$ .

Once an event containing a single signal track is simulated, two sources of background hits are overlaid to its data.

Pile-up collisions are simulated generating events with a variable number of tracks, following the longitudinal beamspot shape described above. To approximately reproduce the LHC Run 3 pile-up conditions, the  $p_T$  distribution for pile-up tracks is tuned to follow what is measured by ATLAS [33], and an average number of simultaneous collisions  $\langle\mu\rangle = 25$  is overlaid to the signal sample.

Random uncorrelated hits are also added in each event to simulate detector noise, matching what is observed in typical ATLAS-simulated samples.

Finally, to emulate the typical Region of Interest (RoI) data selection mechanism adopted for HLT tracking [8], hits are preselected in a wedge with a  $|\Delta\eta| \times |\Delta\phi| = 0.1 \times 0.1$  opening around the signal track, starting from  $\pm 5$  mm around the PV.

Only events that fully contain the signal track are considered to factor out possible acceptance effects for this preselection.

An example event display, where the generated signal track, its corresponding hits and background hits are visible, is shown in Fig. 1.

The data sample adopted for this study contains approximately 400k events for training and 50k events for validation and testing.

### 3. Network Architecture

The task addressed by our GNN-based algorithm is to cluster background hits from pile-up or noise away from hits produced by signal tracks and to cluster separately the signal hits coming from different tracks. For that, we use the condensation approach

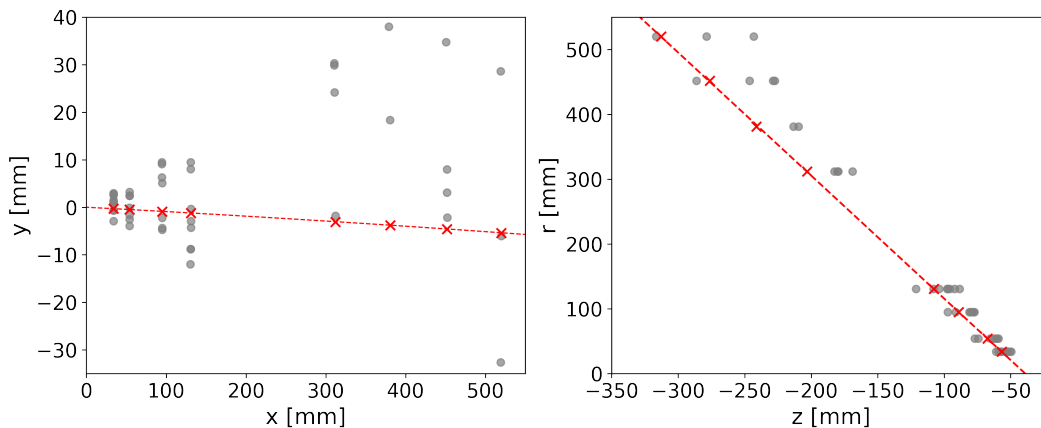


Figure 1: Display of one simulated event in the transverse (left) and longitudinal (right) views with respect to the beam axis. Signal hits are marked in red, pile-up, and noise hits in grey. The dotted line corresponds to the track fitted with a circle in the  $x - y$  plane and a straight line in the  $z - r$  plane.

originally proposed to solve particle flow reconstruction [34, 35] with a few adjustments.

The proposed network is small and compact for demonstration purposes. We use a graph-based approach in which each graph node is a hit parametrized by its position given in Cartesian coordinates, expressed in millimetres. The features are scaled to have a mean of 0 and a standard deviation of 1 for the whole dataset. For simplicity, the graphs are fully connected. This can be generalized later for a larger dataset if the number of edges becomes incompatible with available memory.

The nodes are then passed to the GNN, which consists of 3 blocks:

- **Embedding.** For each node, the input features are transformed into a hidden representation of dimension 5 through an MLP. The dimension was chosen to be as small as possible while preserving performance, considering the subsequent symbolic regression step. For real use cases, this likely will need to be higher.
- **Message Passing (MP).** The hidden representation is passed through the edges as a message to all connecting nodes. For each node, all received messages are summed, concatenated with its hidden representation, and passed through an MLP to update it.
- **Mapping to condensation space.** The updated hidden representations are mapped into the condensation space with dimension 5.

The network has a total of 446 k parameters, which are split approximately equally among the blocks. An illustration is shown in Fig. 2.

To cluster signal and background hits, the loss function consists of attractive and repulsive potentials defined by a separately predicted charge for each node. The charges

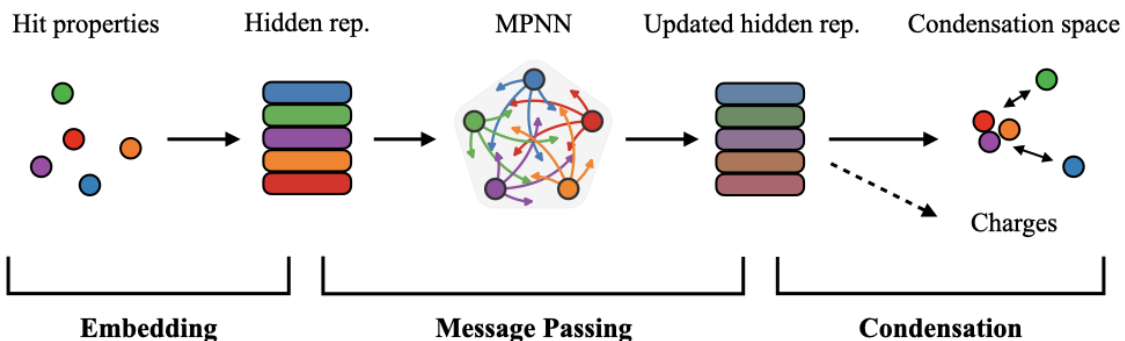


Figure 2: Sketch of the proposed network consisting of three blocks: embedding, message passing and condensation.

are calculated via

$$q_i = \operatorname{arctanh}(\beta_i)^2 + q_{\min} \quad (1)$$

with  $i$  being the node index,  $\beta$  being the output of a separate MLP using the updated hidden representation, and  $q_{\min}$  a hyperparameter optimized to 0.4 through grid search. The loss for the charge prediction is a Binary Cross Entropy (BCE) loss on  $\beta$ , classifying between signal and background hits. The potential for a track  $k$  is then defined by the charge of node  $\alpha$ , which is maximal among the nodes belonging to  $k$ . The attractive and repulsive potentials  $\check{V}_k(x)$  and  $\hat{V}_k(x)$  for node  $k$  with  $x$  being the location in condensation space is given by:

$$\begin{aligned} \check{V}_k(x) &= \|x - x_\alpha\|^2 q_{\alpha k} \\ \hat{V}_k(x) &= \max(0, 1 - \|x - x_\alpha\|) q_{\alpha k} \end{aligned} \quad (2)$$

Where  $\|\cdot\|$  is the L2 norm. We introduce the matrix  $M_{ik}$ , whose elements are set to 1 if node  $i$  belongs to track  $k$  and 0 otherwise, to define the potential loss  $L_V$ :

$$L_V = \frac{1}{N} \sum_{j=1}^N q_j \sum_{k=1}^K \left( M_{jk} \check{V}_k(x_j) + (1 - M_{jk}) \hat{V}_k(x_j) \right) + \frac{1}{N_{noise}} x_j \left( 1 - \sum_{k=1}^K M_{jk} \right) \quad (3)$$

$N$  is the total number of nodes in the event, and  $N_{noise}$  is the number of nodes that do not belong to a track. The first term corresponds to what is proposed in [34]. The second term is added to ensure that the pile-up and noise hits are concentrated near the origin of the condensation space. This significantly simplifies postprocessing, as background rejection can be easily achieved by removing hits condensed in a sphere around the origin.

#### 4. Symbolic Regression

The main goal of this work is to demonstrate that it is possible to approximate the above neural network with a functional expression. For this, we use the symbolic regression algorithm provided through the PYSR package [36].

A first implementation of a symbolic regression approximation to ease FPGA implementation was proposed in [32] in the context of jet classification. There, a single MLP was used to process a set of jet variables. This approach is not suitable for tracking tasks, as our input is set-valued data that can't be processed by a simple MLP.

To overcome this obstacle with a novel approach, we make use of the modularity of the model, which essentially consists of 3 MLPs with a minor processing step in the middle, and we separately replace each MLP with a symbolic expression.

For the embedding network, the function operates uniformly on each node, taking the hit features as input and producing its hidden representation as output.

Given the current choice of fully connected graph, the message-passing step simply sums the hidden representations of all hits. This could change in future implementations, as

an arbitrary graph would require differently masked sums for each hit, depending on its connectivity. Once dealt with this, the MLP of the MP block again acts equally on each node, taking the message as input. For mapping into condensation space, the function takes the updated hidden representation for each node separately and outputs its coordinates similarly to the first block.

We use default PYSR parameters for the SR training. We choose the operators to be  $+$ ,  $-$ ,  $\cdot$ ,  $:$  and  $\text{ReLU}()$  and set the maximal equation length to 75 (150 for the last block). PYSR exhibits a significant decrease in speed for large data sets. To optimize computational resources, we reduce the training dataset to 5,000 hits. In the adopted dataset, only 17% of the hits come from signal tracks. To allow PYSR to learn the signal features correctly, we increase the ratio between signal and background hits to 50% using a random background downscaling.

We iteratively replace the network blocks with learned symbolic expressions, starting with the embedding block. After each replacement, we retrain the rest of the network to reduce performance loss.

## 5. Postprocessing

The proposed GNN model is currently not meant to cover the track reconstruction task completely but rather to produce background hit filtering and track seeding information. So, we implemented some further postprocessing steps leading to a full track reconstruction and fit. Once again, these are kept as simple as possible, as they are only meant to quantify the quality of the seeding and the beneficial impact of background rejection on the combinatorics of the tracking problem.

### 5.1. Hit selection

In the original object condensation proposal, objects are identified based on the charge of the condensation node and everything within a radius around this node is matched with the object. We altered this approach so that it did not depend on the charge prediction for the evaluation as it would require another symbolic replacement, therefore introducing an additional source of error.

Due to the additional term we added to the loss, pile-up and noise hits are ideally clustered at the origin of the condensation space. We can thus remove the background by applying a radius cut around the origin.

In the next step, we apply the MS clustering algorithm to identify the signal hits. This clustering will be crucial for distinguishing hits from different tracks for multi-track datasets. For now, since each event contains just one signal track, it is mainly used to remove further background.

The clustering algorithm has a bandwidth parameter defining the size of the cluster.

Together with the radius cut around the origin, we have two parameters that can be optimized. This is done via grid search for every performance evaluation.

### 5.2. Track reconstruction and fit

After the hit selection, we applied a simplified track reconstruction algorithm inspired by real fast-tracking tasks developed by LHC experiments. For that, we build all possible triplets from the given hits. For each triplet, we construct a circle in the  $x - y$  plane to obtain the track-candidate  $p_T$  and perform a linear fit in the  $z - r$  plane to get  $z_0$ .

These quantities are used to fill a 2D histogram, and triplets within a window around the histogram peak are selected. The window size is dependent on the  $p_T$  of the peak and was chosen large enough to contain all hits if the triplets are built using true signal hits. Only hits from triplets within the chosen window are kept, further improving background rejection.

If, after the above steps, we do not have more than one hit per layer, we perform the final track fit. The fit is performed separately in the  $r - z$  and  $r - \phi$  plane. In  $r - z$ , we fit a straight line using the non-linear least square *curve-fit* method from SCIPY [37]. In the  $r - \phi$  plane, we fit a circle using the *circle-fit* library. If at least one layer contains more than one hit, simplified ambiguity solving is applied. In this case, we perform the linear  $r - z$  fit for each combination and choose the one with the best  $\chi^2$ . This is repeated iteratively for each layer with more than one hit before performing the final circle fit.

## 6. Results

Based on the above-described processing, multiple performance metrics can be evaluated for our models. Results are first presented for the full GNN to show its potential as a tracking tool. This is then used as a baseline to be compared with all the symbolic expression replacement options. We will denote with SR 1 the network with the first stage replaced, with SR 2 the one with both the first and second stages replaced, and with SR 3 the fully approximated network. For SR 1 and SR 2, the evaluations are performed on the retrained network.

As a first figure of merit, we look at the pure condensation output. Fig. 3 shows the condensation radius for signal and background hits for the different models. The performance drop among them is evident through the widening of the peaks.

As already mentioned, the cut-off radius  $r_{\text{cut}}$  and the clustering bandwidth are optimized through grid search for the individual models and are reported in Tab. 1. This shows that to achieve maximum signal efficiency for the clustering step, some loosening of the cut-off radius  $r_{\text{cut}}$  can be needed. In fact, if the distributions for signal and background are not separated enough, the background contamination after a tight radius cut remains too large, possibly leading to the identification of a large cluster that might not contain any



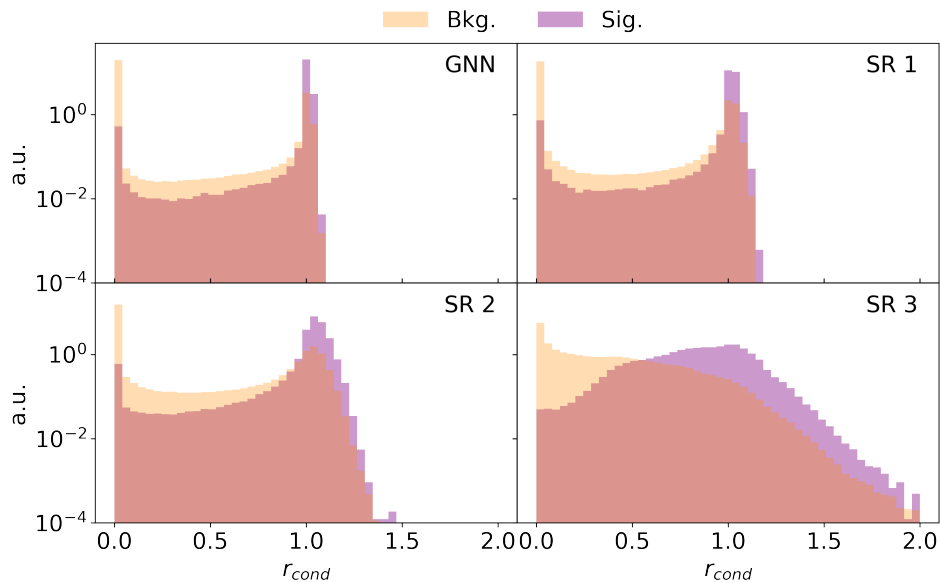


Figure 3: Condensation radius for all signal and background hits for the different stages.

signal hits. This request for a background rejection high enough to obtain a reasonable clustering leads to a  $r_{\text{cut}}$  growth with the number of replaced stages.

We note the signal hit efficiencies ( $\varepsilon_s$ ) and background hit rejections ( $r_b$ ) separately after

	Truth	GNN	SR 1	SR 2	SR 3
$r_{\text{cut}}$	-	0.05	0.2	0.3	0.4
Bandwidth	-	0.7	0.7	0.6	0.7
$\varepsilon_s$ cluster	-	96.3%	94.8%	92.7%	85.5%
$r_b$ cluster	-	93.9%	93.5%	93.0%	71.1%
$\varepsilon_s$ triplets	-	95.0%	93.5%	91.3%	82.4%
$r_b$ triplets	-	98.5%	98.4%	98.2%	90.1%
Hit purity	-	96.8%	95.9%	94.9%	83.3%
$p_T$ fit in $1\sigma$	39.8%	37.8%	37.5%	36.7%	29.7%
$p_T$ fit in $2\sigma$	97.6%	95.0%	94.4%	93.6%	84.5%

Table 1: Clustering parameters and performance metrics. The signal hit efficiencies ( $\varepsilon_s$ ) and background rejections ( $r_b$ ) are measured after the clustering and triplet filtering steps. Hit purity indicates the average percentage of signal hits used in the final best fit after the ambiguity resolution among multiple hit candidates per layer. The track fit performance is evaluated by comparing the fitted  $p_T$  to the true track  $p_T$  and measuring how often their difference is within 1 or 2 times the estimated ideal resolution ( $\sigma$ ). Truth refers to fit results on signal hits only.

clustering and triplet filtering in Tab. 1. The rejection is defined as the percentage of background hits removed by the filtering process. The hit purity after all preprocessing steps, including the ambiguity resolution performed during the fit, defined as the percentage of selected hits that are actually coming from the signal track, is also reported. We emphasize the impact of triplet filtering, which adds about 5 % to the background rejection while losing only slightly more than 1 % on signal efficiency. Comparing the different models, we notice only minor performance losses for SR 1 and SR 2 but a significant drop for SR 3. The hit purity drops by only 2 % for SR 2 with respect to the original GNN and by over 13 % for the full SR model.

The percentage of events in which at least a given number of signal hits is retained after clustering is shown in the left panel of Fig. 4. The fact that the probability of having all 8 signal hits correctly selected is only slightly lower than the individual signal hit efficiency reported in Tab. 1 clearly demonstrates a strong correlation in the misclassification of signal hits. Therefore, the network is much more likely to misclassify a track completely than to identify just part of its hits. This trend can also be seen in the final hit purity distribution, in the right panel of Fig. 4, showing two main peaks at 0 and 100%. The peaks are only slightly smeared out for SR 1 and SR 2, whereas a significant change is observed for SR 3.

We also compare the residuals between the true particle kinematics and those obtained from the final track fit. The results for the  $p_T$  and  $z_0$  track parameters are shown in Fig. 5. Due to the finite detector resolution, even a fit on perfectly selected hits will not give the exact particle features, so residuals of 0 cannot be expected. Thus, we add for reference the results of a fit using only true signal hits, noted as Truth in Fig. 5. As anticipated from previous results, the performance for SR 1 and SR 2 shows very small deviations from the original GNN. If the signal hit filtering fails completely, the circle fit gives a nearly null  $p_T$  estimate, leading to a small peak around 1 in the normalized

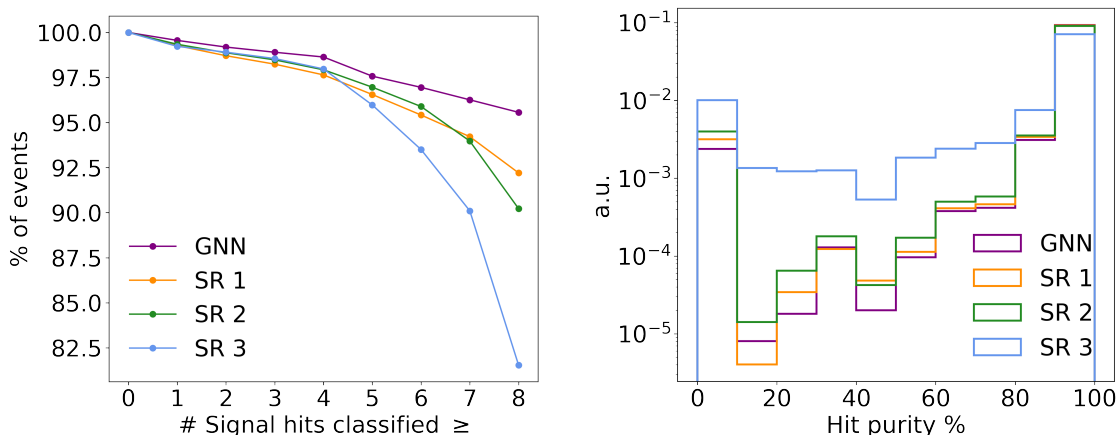


Figure 4: Percentage of events with  $\geq N$  signal hits selected after clustering (left). Percentage of signal in the hits selected for the final track fit (right).

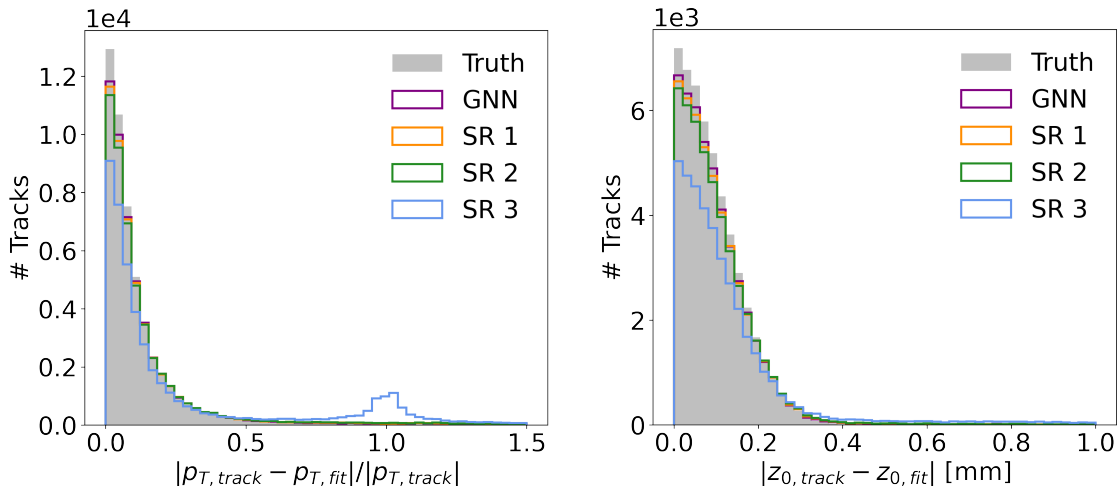


Figure 5: Residual of fitted track features. Normalized  $p_T$  residual (left) and  $z_0$  (right).

residual distribution.

To quantify how  $p_T$  fit residuals behave in the different models, they are compared to the expected ideal resolution. This, in turn, depends on  $p_T$ , as a high-energy track with little curvature is more sensitive to a perturbation of its hit positions due to finite detector resolution than a low-energy track. Taking this into account, to get a rough estimate of the ideal  $p_T$  resolution, we divide the data into bins of true track  $p_T$  and fit a Gaussian to the truth fit residuals for each bin, extracting  $\sigma$ . This allows us to measure the percentage of full track fits for which the  $p_T$  residuals fall into the  $1\sigma$  or  $2\sigma$  range. Such results are shown at the bottom of Tab. 1.

We acknowledge that this approach suffers from several limitations, such as the freedom of choice for the  $p_T$  binning, low statistics in the high-energy range, and the Gaussian not being a good approximation for high  $p_T$  regions due to one-sided tails. However, we believe it to be sufficient for the proof-of-concept presented here. A more solid approach will be implemented in future work, based on including the hit position uncertainties in the fit to extract an uncertainty on each fitted parameter.

A possible application of the proposed network is to cut away background hits to reduce the combinatorics of the tracking problem significantly. This benefit can be quantified by counting the number of constructed triplets after hit filtering with the different models. To give a rough estimate, an ideal selection retaining only 8 signal hits would lead to 56 triplets. For the full GNN, SR 1 and SR 2, we count on average around 100 triplets, while for SR 3, the average triplet number is close to 1000. These numbers must be compared to the average triplet count obtained without any filtering, which is around 13000. This demonstrates that even a limited background rejection (around 70% for the SR 3 case) can grant more than a factor of 10 timing improvement for triplet processing. Such a conclusion will be considered for future studies, optimizing the network to prioritise signal efficiency over background rejection.

## 7. Conclusion

In this work, we presented a new approach utilizing symbolic regression to approximate complex neural networks for fast inference and feasible implementation on FPGAs. Starting with a graph neural network, we split the model into its three MLP components and found an analytical function for each.

The goal is to demonstrate that adopting symbolic approximations can ease the implementation of such or similar networks for track-finding in the trigger system. In fact, while fast machine learning packages like HLS4ML [38] can be used to implement a neural network on FPGAs, their resources saturate for a network with more than 10k parameters. A symbolic function is, therefore, easier to implement.

We find that replacing the first two MLP blocks leads to minor performance losses, and only replacing the last layer causes a significant drop in performance. The method we propose is anyway flexible enough to allow deciding whether to replace everything with symbolic regression or only the first blocks and keep a small network for the last step to minimize performance loss.

Furthermore, the question can be posed as to what the goal of the network should be. In this paper, we used the network for track seeding, implementing an external postprocessing composed of clustering and final track-fitting. However, the network can also be used as a pre-filtering step to reduce combinatorics and speed up conventional track-finding algorithms.

The feasibility of both approaches has to be studied after generalizing to more realistic datasets with multiple tracks. Further investigations will also include the implementation on FPGAs and timing studies.

## Acknowledgement

NS and EG are supported by the BSF-NSF grant 2028 and the ISF Research Center 494.

## References

- [1] ATLAS Collaboration. “The ATLAS Experiment at the CERN Large Hadron Collider”. In: *JINST* 3 (2008), S08003. DOI: [10.1088/1748-0221/3/08/S08003](https://doi.org/10.1088/1748-0221/3/08/S08003).
- [2] CMS Collaboration. “The CMS Experiment at the CERN LHC”. In: *JINST* 3 (2008), S08004. DOI: [10.1088/1748-0221/3/08/S08004](https://doi.org/10.1088/1748-0221/3/08/S08004).
- [3] Lyndon Evans and Philip Bryant. “LHC Machine”. In: *JINST* 3 (2008), S08001. DOI: [10.1088/1748-0221/3/08/S08001](https://doi.org/10.1088/1748-0221/3/08/S08001).
- [4] Georges Aad et al. “Operation of the ATLAS trigger system in Run 2”. In: *JINST* 15.10 (2020), P10004. DOI: [10.1088/1748-0221/15/10/P10004](https://doi.org/10.1088/1748-0221/15/10/P10004). arXiv: [2007.12539](https://arxiv.org/abs/2007.12539) [[physics.ins-det](#)].
- [5] Georges Aad et al. “The ATLAS Trigger System for LHC Run 3 and Trigger performance in 2022”. In: (Jan. 2024). arXiv: [2401.06630](https://arxiv.org/abs/2401.06630) [[hep-ex](#)].
- [6] Vardan Khachatryan et al. “The CMS trigger system”. In: *JINST* 12.01 (2017), P01020. DOI: [10.1088/1748-0221/12/01/P01020](https://doi.org/10.1088/1748-0221/12/01/P01020). arXiv: [1609.02366](https://arxiv.org/abs/1609.02366) [[physics.ins-det](#)].
- [7] Elisa Fontanesi. *New trigger strategies for CMS during Run 3*. Tech. rep. Geneva: CERN, 2022. DOI: [10.22323/1.414.0681](https://doi.org/10.22323/1.414.0681). URL: <https://cds.cern.ch/record/2842439>.
- [8] ATLAS Collaboration. “The ATLAS inner detector trigger performance in  $pp$  collisions at 13 TeV during LHC Run 2”. In: *Eur. Phys. J. C* 82 (2022), p. 206. DOI: [10.1140/epjc/s10052-021-09920-0](https://doi.org/10.1140/epjc/s10052-021-09920-0). arXiv: [2107.02485](https://arxiv.org/abs/2107.02485) [[hep-ex](#)].
- [9] Andreas Salzburger et al. *TrackML Particle Tracking Challenge*. 2018. URL: <https://kaggle.com/competitions/trackml-particle-identification>.
- [10] Sabrina Amrouche et al. “The Tracking Machine Learning challenge : Accuracy phase”. In: *The NeurIPS '18 Competition: From Machine Learning to Intelligent Conversations*. Apr. 2019. DOI: [10.1007/978-3-030-29135-8\\_9](https://doi.org/10.1007/978-3-030-29135-8_9). arXiv: [1904.06778](https://arxiv.org/abs/1904.06778) [[hep-ex](#)].
- [11] Javier Duarte and Jean-Roch Vlimant. “Graph Neural Networks for Particle Tracking and Reconstruction”. In: (Dec. 2020). DOI: [10.1142/9789811234033\\_0012](https://doi.org/10.1142/9789811234033_0012). arXiv: [2012.01249](https://arxiv.org/abs/2012.01249) [[hep-ph](#)].
- [12] Lukas Heinrich et al. “Combined track finding with GNN & CKF”. In: Jan. 2024. arXiv: [2401.16016](https://arxiv.org/abs/2401.16016) [[hep-ex](#)].
- [13] Gage DeZoort et al. “Charged Particle Tracking via Edge-Classifying Interaction Networks”. In: *Comput. Softw. Big Sci.* 5.1 (2021), p. 26. DOI: [10.1007/s41781-021-00073-z](https://doi.org/10.1007/s41781-021-00073-z). arXiv: [2103.16701](https://arxiv.org/abs/2103.16701) [[hep-ex](#)].
- [14] Daniel Murnane, Savannah Thais, and Ameya Thete. “Equivariant Graph Neural Networks for Charged Particle Tracking”. In: *21th International Workshop on Advanced Computing and Analysis Techniques in Physics Research: AI meets Reality*. Apr. 2023. arXiv: [2304.05293](https://arxiv.org/abs/2304.05293) [[physics.ins-det](#)].

- [15] Ryan Liu et al. “Hierarchical Graph Neural Networks for Particle Track Reconstruction”. In: *21th International Workshop on Advanced Computing and Analysis Techniques in Physics Research: AI meets Reality*. Mar. 2023. arXiv: [2303.01640 \[hep-ex\]](#).
- [16] Catherine Biscarat et al. “Towards a realistic track reconstruction algorithm based on graph neural networks for the HL-LHC”. In: *EPJ Web Conf.* 251 (2021), p. 03047. DOI: [10.1051/epjconf/202125103047](#). arXiv: [2103.00916 \[physics.ins-det\]](#).
- [17] Savannah Thais and Gage DeZoort. “Instance Segmentation GNNs for One-Shot Conformal Tracking at the LHC”. In: *34th Conference on Neural Information Processing Systems*. Mar. 2021. arXiv: [2103.06509 \[cs.CV\]](#).
- [18] A. Bocci et al. “Heterogeneous Reconstruction of Tracks and Primary Vertices With the CMS Pixel Tracker”. In: *Frontiers in Big Data* 3 (2020). ISSN: 2624-909X. DOI: [10.3389/fdata.2020.601728](#). URL: <https://www.frontiersin.org/articles/10.3389/fdata.2020.601728>.
- [19] Javier Duarte et al. “Fast inference of deep neural networks in FPGAs for particle physics”. In: *JINST* 13.07 (2018), P07027. DOI: [10.1088/1748-0221/13/07/P07027](#). arXiv: [1804.06913 \[physics.ins-det\]](#).
- [20] Javier Duarte et al. “Fast inference of deep neural networks in FPGAs for particle physics”. In: *JINST* 13.07 (2018), P07027. DOI: [10.1088/1748-0221/13/07/P07027](#). arXiv: [1804.06913 \[physics.ins-det\]](#).
- [21] Vladimir Loncar et al. “Compressing deep neural networks on FPGAs to binary and ternary precision with HLS4ML”. In: *Mach. Learn. Sci. Tech.* 2 (2021), p. 015001. DOI: [10.1088/2632-2153/aba042](#). arXiv: [2003.06308 \[cs.LG\]](#).
- [22] Chang Sun et al. “Fast muon tracking with machine learning implemented in FPGA”. In: *Nucl. Instrum. Meth. A* 1045 (2023), p. 167546. DOI: [10.1016/j.nima.2022.167546](#). arXiv: [2202.04976 \[physics.ins-det\]](#).
- [23] Thea Aarrestad et al. “Fast convolutional neural networks on FPGAs with hls4ml”. In: *Mach. Learn. Sci. Tech.* 2.4 (2021), p. 045015. DOI: [10.1088/2632-2153/ac0ea1](#). arXiv: [2101.05108 \[cs.LG\]](#).
- [24] Anders Ryd and Louise Skinnari. “Tracking Triggers for the HL-LHC”. In: *Ann. Rev. Nucl. Part. Sci.* 70 (2020), pp. 171–195. DOI: [10.1146/annurev-nucl-020420-093547](#). arXiv: [2010.13557 \[physics.ins-det\]](#).
- [25] Aneesh Heintz et al. “Accelerated Charged Particle Tracking with Graph Neural Networks on FPGAs”. In: *34th Conference on Neural Information Processing Systems*. Nov. 2020. arXiv: [2012.01563 \[physics.ins-det\]](#).
- [26] Abdelrahman Elabd et al. “Graph Neural Networks for Charged Particle Tracking on FPGAs”. In: *Front. Big Data* 5 (2022), p. 828666. DOI: [10.3389/fdata.2022.828666](#). arXiv: [2112.02048 \[physics.ins-det\]](#).

- [27] Yutaro Iiyama et al. “Distance-Weighted Graph Neural Networks on FPGAs for Real-Time Particle Reconstruction in High Energy Physics”. In: *Front. Big Data* 3 (2020), p. 598927. DOI: [10.3389/fdata.2020.598927](https://doi.org/10.3389/fdata.2020.598927). arXiv: [2008.03601](https://arxiv.org/abs/2008.03601) [[physics.ins-det](#)].
- [28] Zhixing Jiang et al. “Ultra Fast Transformers on FPGAs for Particle Physics Experiments”. In: (Feb. 2024). arXiv: [2402.01047](https://arxiv.org/abs/2402.01047) [[cs.LG](#)].
- [29] Anja Butter et al. “Back to the formula - LHC edition”. In: *SciPost Phys.* 16.1 (2024), p. 037. DOI: [10.21468/SciPostPhys.16.1.037](https://doi.org/10.21468/SciPostPhys.16.1.037). arXiv: [2109.10414](https://arxiv.org/abs/2109.10414) [[hep-ph](#)].
- [30] Shehu AbdusSalam, Steven Abel, and Miguel Crispim Romão. “Symbolic Regression for Beyond the Standard Model Physics”. In: (May 2024). arXiv: [2405.18471](https://arxiv.org/abs/2405.18471) [[hep-ph](#)].
- [31] Tanner Mengel et al. “Interpretable machine learning methods applied to jet background subtraction in heavy-ion collisions”. In: *Phys. Rev. C* 108.2 (2023), p. L021901. DOI: [10.1103/PhysRevC.108.L021901](https://doi.org/10.1103/PhysRevC.108.L021901). arXiv: [2303.08275](https://arxiv.org/abs/2303.08275) [[hep-ex](#)].
- [32] Ho Fung Tsoi et al. “Symbolic Regression on FPGAs for Fast Machine Learning Inference”. In: *EPJ Web Conf.* 295 (2024), p. 09036. DOI: [10.1051/epjconf/202429509036](https://doi.org/10.1051/epjconf/202429509036). arXiv: [2305.04099](https://arxiv.org/abs/2305.04099) [[cs.LG](#)].
- [33] ATLAS Collaboration. “Charged-particle distributions in  $\sqrt{s} = 13$  TeV  $pp$  interactions measured with the ATLAS detector at the LHC”. In: *Phys. Lett. B* 758 (2016), p. 67. DOI: [10.1016/j.physletb.2016.04.050](https://doi.org/10.1016/j.physletb.2016.04.050). arXiv: [1602.01633](https://arxiv.org/abs/1602.01633) [[hep-ex](#)].
- [34] Jan Kieseler. “Object condensation: one-stage grid-free multi-object reconstruction in physics detectors, graph and image data”. In: *Eur. Phys. J. C* 80.9 (2020), p. 886. DOI: [10.1140/epjc/s10052-020-08461-2](https://doi.org/10.1140/epjc/s10052-020-08461-2). arXiv: [2002.03605](https://arxiv.org/abs/2002.03605) [[physics.data-an](#)].
- [35] Shah Rukh Qasim et al. “End-to-end multi-particle reconstruction in high occupancy imaging calorimeters with graph neural networks”. In: *Eur. Phys. J. C* 82.8 (2022), p. 753. DOI: [10.1140/epjc/s10052-022-10665-7](https://doi.org/10.1140/epjc/s10052-022-10665-7). arXiv: [2204.01681](https://arxiv.org/abs/2204.01681) [[physics.ins-det](#)].
- [36] Miles Cranmer. *Interpretable Machine Learning for Science with PySR and SymbolicRegression.jl*. 2023. arXiv: [2305.01582](https://arxiv.org/abs/2305.01582) [[astro-ph.IM](#)].
- [37] Pauli Virtanen et al. “SciPy 1.0: Fundamental Algorithms for Scientific Computing in Python”. In: *Nature Methods* 17 (2020), pp. 261–272. DOI: [10.1038/s41592-019-0686-2](https://doi.org/10.1038/s41592-019-0686-2).
- [38] FastML Team. *fastmachinelearning/hls4ml*. Version v0.8.1. 2023. DOI: [10.5281/zenodo.1201549](https://doi.org/10.5281/zenodo.1201549). URL: <https://github.com/fastmachinelearning/hls4ml>.